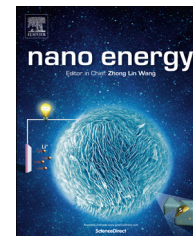


Available online at www.sciencedirect.com

ScienceDirect

journal homepage: www.elsevier.com/locate/nanoenergy

RAPID COMMUNICATION

High-throughput fabrication of strutted graphene by ammonium-assisted chemical blowing for high-performance supercapacitors

Xiang-Fen Jiang^{a,1}, Xue-Bin Wang^{a,b,c,*}, Pengcheng Dai^a, Xia Li^a,
Qunhong Weng^{a,**}, Xi Wang^{b,***}, Dai-Ming Tang^{a,b}, Jie Tang^d,
Yoshio Bando^a, Dmitri Golberg^a

^aWorld Premier International Center for Materials Nanoarchitectonics (WPI-MANA), National Institute for Materials Science (NIMS), Namiki 1-1, Tsukuba 305-0044, Japan

^bInternational Center for Young Scientists (ICYS), NIMS, Tsukuba 305-0044, Japan

^cCollege of Engineering and Applied Sciences, Nanjing University, Nanjing 210093, China

^d1D Nanomaterials Group, NIMS, Sengen 1-2-1, Tsukuba 305-0047, Japan

Received 1 May 2015; received in revised form 15 June 2015; accepted 15 June 2015

KEYWORDS

Three dimensional graphene;
Strutted graphene;
Chemical blowing;
Supercapacitor

Abstract

Three dimensional graphenes are most desired to deliver the unique nano-sized properties of graphenes to the macro-scale, yet their practical production remains insufficient. Herein we establish a general synthesis approach, *i.e.* ammonium-assisted chemical blowing *via* foaming sucrose into the bubble networks of sucrose-derived polymers, to effectively produce three dimensional strutted graphenes (SGs). SG consists of interconnected mono-/few-layered graphene membranes scaffolded by graphitic struts without restacking or agglomeration, which thus fully exposes the huge surface and possesses appropriate porosity. The SG is further

*Corresponding author at: World Premier International Center for Materials Nanoarchitectonics (WPI-MANA), National Institute for Materials Science (NIMS), Namiki 1-1, Tsukuba 305-0044, Japan.
Tel.: +81 298513354 ext.8814.

**Corresponding author.

***Corresponding author.

E-mail addresses: WANGXB@fuji.waseda.jp,
WANG.Xuebin@nims.go.jp (X.-B. Wang),
WENG.Qunhong@nims.go.jp (Q. Weng),
WANG.Xi2@nims.go.jp (X. Wang).

¹These authors contributed equally.

<http://dx.doi.org/10.1016/j.nanoen.2015.06.008>
2211-2855/© 2015 Elsevier Ltd. All rights reserved.

applied as additive/binder-free electrodes for supercapacitors, which realize the high energy density of 50 W h kg^{-1} and the high maximum-power-density of 340 kW kg^{-1} due to the large surface area, excellent interconnectivity and porosity. The mass-produced self-supporting SG would open up a wide horizon and enable the abundant potentials of graphenes for promising large-scale applications.

© 2015 Elsevier Ltd. All rights reserved.

Introduction

Supercapacitors, especially electrical double layer capacitors (EDLC), are promising energy storage devices for pulse charge/discharge and high power supply with 1 million cycle lifetime and low maintenance cost, which benefit from the rapid reversible adsorption and desorption of ions in porous electrodes [1]. Activated carbons have been dominantly used in industry as supercapacitor electrodes for their good conductivity, surface area, stability and low cost [2], although they suffer from the slow kinetics of ion transports in their small pores. Recently, graphenes have been widely explored as supercapacitor electrodes, yet their performances are also limited by sluggish ion and electron transports due to the narrow channels of aggregated graphenes and contact resistances respectively. And the ion-accessible surfaces are reduced owing to the re-stacking of graphenes. Three dimensional (3D) graphenes could effectively provide interconnected architectures without those drawbacks, hence to actualize graphene-based energy storage as well as to simplify the device fabrication from a practical viewpoint [3–5].

Currently, the blooming 3D graphenes have been produced generally in three types: assembly of reduced graphene oxide (RGO), foams directed by chemical vapor deposition (CVD) and polymer-derived architectures. RGO hydrogels or aerogels were accomplished by the 3D assembly of graphene oxide coupled with simultaneous or subsequent reduction, by means of hydrothermal gelation [6–8], chemical reduction gelation [9], freeze-drying [10,11], solvent-mediated capillary compression [12,13], casting [14,15], filtration [16–18], breath figure lithography [19], 3D print [20,21], sacrificial templating [22–25], and functional linker/spacer/scaffold-incorporated assembly with organics [26–28], metals [29–31], nickel foams [32,33], carbon nanotubes [34–41], pyrolytic carbons [42], mesoporous carbons [43,44], or carbon weaves [45,46]. 3D graphene foams could be directed by templates, e.g. nickel foams, in CVD processes [47–49]. The polymer-derived 3D graphene architectures, strutted graphenes (SG) distinctively integrating continual graphitic struts and membranes, were recently developed via the sugar-blowing route [50]. The SG-based aqueous supercapacitors demonstrated the extremely high maximum-power of 1000 kW kg^{-1} . However, the synthesis route succeeding only based on glucose precursors needs to be extended to a general strategy for practical production of SG, and the aqueous supercapacitors with low operation voltage of 1 V and low energy density around 8 W h kg^{-1} needs to be improved [50].

Inspired by our previous work on the self-chemical-blowing method for making boron nitride foams [51] and

the sugar-blowing method for making SG [50], herein we propose a general concept, *i.e.* ammonium-assisted chemical blowing, as the universal strategy for making SG. Ammonium-assisted chemical blowing relies on the polymers deriving from diverse sugar precursors such as sucrose and even household sugars coupling with the blowing agents of decomposable residue-free ammonium salts. It is capable of producing cost-effective SG on a large scale. The SG is further directly applied to supercapacitors in organic electrolytes to realize a high energy density of 50 W h kg^{-1} , by improving the operation voltage. In addition, the additive/binder-free SG-based supercapacitors sustain the high maximum-power-density of 340 kW kg^{-1} in the organic electrolyte, taking advantages of large surface area, multi-dimensional electron transport pathways, and minimized resistance of ion transports within bubble cavities of the SG. The electrochemically stable high-performance SG-based supercapacitors thus enable their admirable applications of quick discharging such as the instantaneous startup of electric vehicles.

Experimental section

Sucrose (Wako Chemical Co.) or household sugars was directly mixed with NH_4Cl and $(\text{NH}_4)_2\text{CO}_3$ with the mass ratio 1:1:1 and heated in a horizontal furnace to 1400°C at a heating rate of 4°C min^{-1} and annealed for 3 h under Ar atmosphere. The exhaust was cooled by water to deposit the ammonium salts. The morphology of products was characterized by a scanning electron microscope (SEM, Hitachi S-4800) and a high-resolution transmission electron microscope (HRTEM, JEOL JEM-3000F). The structures were characterized by electron energy loss spectroscopy (EELS, attachment of JEOL JEM-3000F), X-ray diffraction (XRD, Rigaku Ultima III) and Raman spectroscopy (HORIBA Jobin Yvon T6400). The composition was characterized by an X-ray photoelectron spectroscopy (XPS, Thermo Scientific Escalab 250Xi) after Ar^+ ion bombardment for 10 s. Nitrogen adsorption-desorption measurements were carried out at a liquid nitrogen temperature on Quantachrome Autosorb-1.

The SG-based supercapacitors were constructed of symmetric electrodes. The SG was tailored into pieces of 1 mg using a scissor, which were attached into 200 mesh steel grid collectors by folding four corners of steels. The two electrodes were immersed into 1 M tetraethylammonium tetrafluoroborate (TEABF_4)/acetonitrile (AN) solution with the separators of 20 mesh cotton to construct a cell under the packaging pressure of 500 Pa. Neither binders nor additives were used here.

Electrochemistry tests of SG-based supercapacitors were done by workstations of Solartron 1280B (Solartron Co.) and VersaSTAT 4 (Princeton Applied Research), including cyclic voltammetry (CV), chronopotentiometry and electrochemical impedance spectrometry (EIS) referring to the open circuit voltage (OCV). Gravimetric specific capacitance, C , was calculated from galvanostatic charging/discharging using

$$C = \frac{4I}{m(dV/dt)} \quad (1)$$

where I is the constant current when discharging; m is the mass of SG in both electrodes; dV/dt is the slope of linear parts on discharge curves. Direct current (DC) internal resistance, $R_{i,DC}$, is obtained in potentiostatic charging and subsequent galvanostatic discharging (Note that here it is not multi-step galvanostatic charging/discharging) by:

$$R_{i,DC} = \frac{V_{drop}}{I} \quad (2)$$

where V_{drop} is the initial voltage drop at the very beginning of discharging. The potentiostatic-charging/galvanostatic-discharging was supplied by Saltron workstation; and the terminal voltage of the cell was separately monitored by Princeton workstation to avoid any switch time delay of workstations. The step time for completely building up the designed galvanostatic-discharging currents was ca. 1.1 ms, when the voltage drop was defined as V_{drop} . Equivalent series resistance (ESR) was determined from the x-intercept of the Nyquist plot of EIS. Equivalent parallel resistance (ERR) was calculated as the ratio of voltage and current after conducting potentiostatic tests for 5 min. The stored energy density, E , was calculated by:

$$E = \frac{CV^2}{8} \quad (3)$$

where V is the operation voltage of cells, 2.7 V. The maximum discharge peak power density, P_m , is an intrinsic parameter for the comparison among different capacitors, determined by:

$$P_m = \frac{V_{OCV}^2}{4mR_{i,DC}} \quad (4)$$

Results and discussion

Characterizations and properties of SG

The SG products are sponge-like solid foams (the inset of Figure 1a). They are produced in high throughput of ca. 100 mg every run via the ammonium-assisted chemical blowing route. The yield rate of SG is 10-20 wt% with respect to sucrose. In the synthesis, the polymers derived from heating sucrose or household sugars were blown into crowded bubble networks by the gases from ammonium blowing agents. These polymer bubbles were further converted into the polyhedral configuration encircled by graphene membranes and braced by graphite struts after annealing, *i.e.* SG, as shown in Figure 1a. The connecting regions of three or four bubbles are named as struts in foam subdiscipline (Figure 1b), which serve as glues for

structurally intimate interconnectivity of graphene membranes in the whole architecture, and as scaffolds for supporting huge-surface graphene membranes for preventing the restacking. The few-layered graphene membranes are fully occupied on surfaces by the ripples with the fluctuation amplitude of 10-100 nm (Figure 1c), and they are thin in thickness to demonstrate the unique graphene properties (Figure 1d). The ripples might result from the thermodynamic relaxation such as the contraction due to surface tension and high-elastic deformation of sugar-derived polymers at the ending of blowing process, which also prohibit from the restacking. In addition, some stomalike pores with diameters around 1 μ m are clearly seen within struts (Figure 1e, f). Actually the stomata appeared in struts before the annealing, possibly resulting from the secondary gas puffing in the ending of the curing of polymers. The stomata decrease the fraction of struts in SG, emphasize the surface area deriving from graphene membranes in SG, and thus ensure the high surface area of whole SG regardless of the micron-level thick struts. The bulk density of the SG is 3-10 mg cm⁻³, the porosity of which is thus calculated to be 99.5-99.8%.

Individual graphene membranes are transferred onto substrates, taking large lateral dimensions with tens of micron (Figure 2a, b). The mono-/few-layered graphenes with clear straight edges of 1-2 and 3-4 layers are shown in the HRTEM images (Figure 2c, d). Some concavities and sparse holes (1-10 nm) circled by (002) crystal planes are seen in the graphene membranes. They might be caused by the loss of some volatile species and the etching to amorphous carbon in the high-temperature annealing. The abundant edges of such concavity and hole structures highly contribute to the additional ultra-high surface area. In the Raman profile of graphene membranes, the sharp 2D peak has full width at half maximum (FWHM) of 55 cm⁻¹ and half of the intensity of the G peak, probably evidencing the well graphitized few-layers [52]. The strong D peak indicates the massive defects such as domain boundaries and edge states.

The crystalline and elemental analyses of SG were further studied. In XRD (Figure 3a), the (002) peak locates at 25.8° with the d value of 0.345 nm. The lattice parameters are refined to be $a=0.252(2)$ nm, $c=0.6906(4)$ nm, slightly larger than the standard graphite (JCPDS 41-1487, $a=0.24704$ nm, $c=0.67244$ nm). Although the spacing of (002) crystal planes is close to that of turbostratic graphitic structures, the graphitization of SG is still good enough for electron transports in our opinion, especially considering that the (002) spacing of graphenes becomes larger at smaller layers [53,54]. The conductivity of the whole SG is measured as 0.5-2 S m⁻¹. In EELS sensitive to light elements (Figure 3b), only clear carbon K-edge feature appears with neither nitrogen nor oxygen ones, indicating the rare impurities. The first and second peaks correspond to the transitions from 1s to π^* and σ^* respectively. The four fine structures i-iv are affirmatively identified although they cannot be distinctly separated owing to the noise, which is the clear characteristic of sp^2 hybridized carbon [55]. The ratio $sp^2/(sp^2+sp^3)$ of our SG is determined as high as 94% according to Cuomo's method in supposing only sp^2 bonding in the reference graphite [56,57]. The high elemental purity of SG is further confirmed by the survey of XPS with only carbon signals (Figure 3c). SG contains less than 2 at%

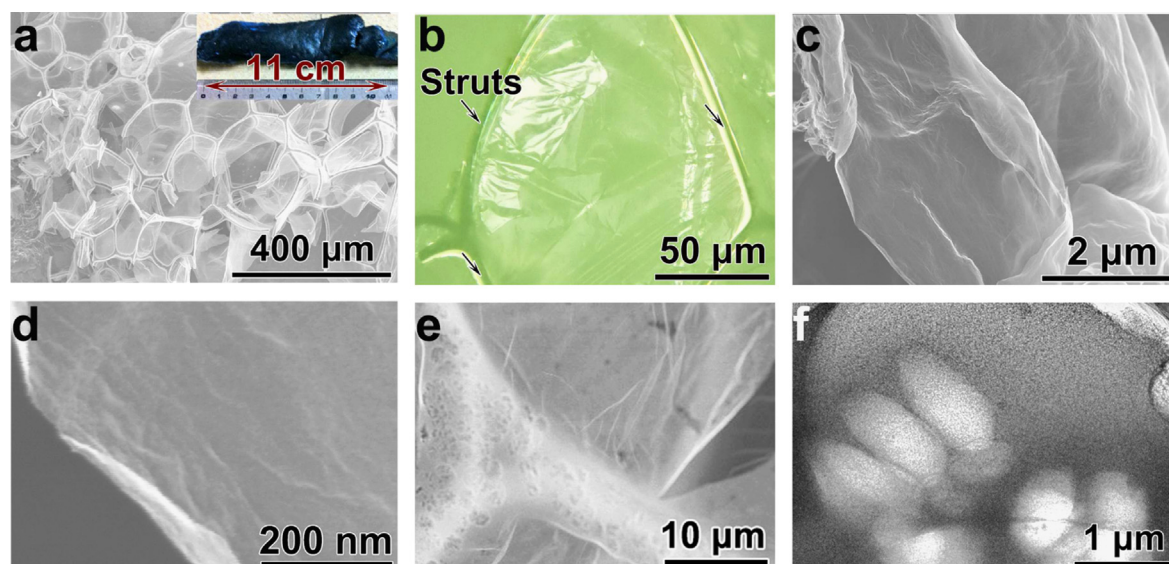


Figure 1 Membrane and strut structures of SG. (a) Photograph and SEM image of the produced SG. (b) Optical image of a graphene membrane enclosed by 4 graphitic struts in the SG. (c, d) SEM image of a huge graphene membrane and the high-resolution image of its surface full of nanosized ripples. (e, f) SEM and TEM images of struts with stoma-like structures.

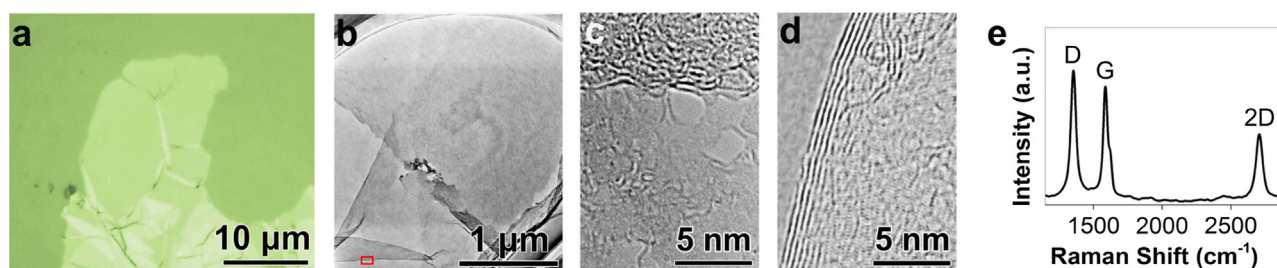


Figure 2 Structures of mono-/few-layered graphene membranes. (a) Optical image of an individual large-area few-layered graphene membrane on a SiO₂/Si substrate. (b) TEM survey of a graphene membrane suspended upon holey carbon mesh. (c) HRTEM image of a 2-4 layered graphene crossing over a 1-2 layered one with some concave and hole structures attached on the surface, taken from the marked region of (b). Both the amount and the size of original holes increased under the irradiation of TEM. The crystalline status was also somewhat deteriorated by electron irradiation. (d) HRTEM image of a 5-layered graphene membrane with the (002) plane spacing of 0.35 nm. (e) Raman spectrum of the graphene membrane.

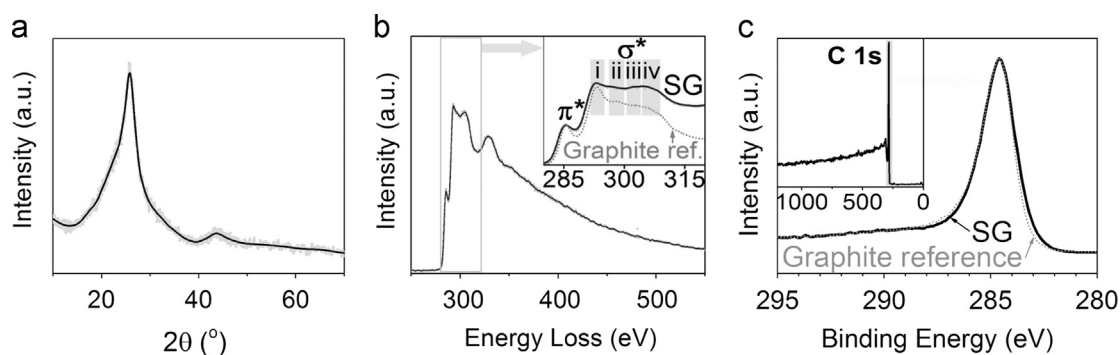


Figure 3 Crystalline and elemental characterizations of SG. (a) XRD, (b) EELS and (c) XPS profiles of SG with graphite references, reflecting the dominant sp^2 hybridization and the high elemental purity.

nitrogen and oxygen impurities in the further fine element scans of XPS. The well graphitization level is confirmed by the FWHM of XPS C1s peak, 1.89 eV, close to that of the reference graphite [58].

The SG architectures have hierarchical porous structures: closely-packed bubble networks, ripples and concaves attached on membranes, and stomata in struts. Graphene membranes are prohibited from re-stacking and

agglomeration by the supporting effect of the struts of bubble networks, so they dominate the large specific surface area (SSA) of SG to be $710 \text{ m}^2 \text{ g}^{-1}$ based on the Brunauer Emmett Teller (BET) equation. On the contrary, the disintegrated SG product (denoted as D-SG) by an ultrasonic disintegrator has the lower SSA of $500 \text{ m}^2 \text{ g}^{-1}$. As shown in Figure 4a, SG has a type IV isotherm characterized by a hysteresis loop and the unsaturated adsorption near saturation vapor pressure. The hysteresis loop of SG resembles type H3 capillaries with open ends in the classification of International Union of Pure and Applied Chemistry (IUPAC). The adsorption branch of the hysteresis loop is featured by two steep increases, *i.e.* twice quick capillary condensations C1 and C2. In the pore distribution (Figure 4b), C1 appears both in adsorption and desorption indicating the substantial inartificial signal. It locates at 4.0 and 4.7 nm depending on Barret Joyner Halenda (BJH) theory and quenched solid density function (QSDFT) theory using the model of slit/cylinder pores at 77 K respectively. The BJH theory usually underestimates the pore sizes by *ca.* 20%. C1 results from the concaves in membranes as well as some mesopores in struts. The etching of amorphous carbon in annealing may cause mesopores in struts, although they are not visually distinguished owing to the large thickness of the struts. The width of C2-related pores is estimated to be 50 and 30 nm according to BJH and QSDFT theories respectively. Actually neither Kelvin equation of the BJH method nor QSDFT method can work well for calculating the sizes of such large pores. C2 relates to the ripples/stomata structures of SG which in D-SG was destroyed by the ultrasonic; therefore C2 clearly disappears in both the isotherm and the pore distribution of D-SG, resulting in the lower SSA.

In the further analysis of the cumulative SSA and pore volume (Figure 4c), the contributions of micropores to both SSA and pore volume are rather limited. 2-10 nm pores contribute the main SSA of SG. The pores with the sizes larger than 10 nm contribute a little to SSA, but significantly more to the pore volume in SG than that in D-SG, because the pore volume of D-SG highly decreases due to the agglomeration in ultrasonic. Note that the pore volume analyzed by the physisorption tests is the only nanopore parts except macroscopic-sized pores of specimens owing to the limited condensation of nitrogen. The SG has very high porosity as indicated by its bulk density. The

macropore-involved porosity and high SSA of SG are beneficial for quick electrolytic ion transports in supercapacitors.

Growth process of ammonium-assisted chemical blowing for SG

The intermediates in the ammonium-assisted chemical blowing are the mixture of diverse sugar-derived polymers, mainly melanoidin and its analogs [50]. The intermediates have bubble-like structures (Figure 5a), featuring our “blowing” mechanism. When heating sucrose with ammonium salts, the released gases from the decomposition of ammonium salts blew the melting syrup into the bubbles. Along with the gradually increased viscosity and decreased plasticity due to the polymerization of sugars, the foam of crowded bubbles of sugar-derived polymers was formed and kept. The walls of polymer bubbles were thinned by the bubble volume dilatation forced by released gas and by the drainage of polymer fluids out of walls into struts driven by surface tension. The polymer bubbles thus have thin walls down to *ca.* 20 nm (Figure 5b, c). Both the small thickness and the interior stresses of polymer walls due to the dilatation would introduce the orientation of polymer molecules along the walls [59], which further leads to the easier carbonization and graphitization of the thermosetting polymer walls for graphene membranes. Meanwhile, the carbon fragments are eliminated to further decrease the thickness of the walls and to achieve the mono-/few-layered graphene membranes in the final high-temperature annealing.

In heating sucrose and ammonium salts to *ca.* 250 °C, the mixture becomes complex polymers with small amount of residual ammonium chloride corresponding to the peak at 3050 cm^{-1} in Figure 5d. The sugar-derived polymers demonstrate gradually increased conjugated system in further heating as reflected by the vibration at 1585 cm^{-1} , which finally approach the graphitic configuration. The sugar-derived polymers taken around 300 °C are specified to be $\text{C}_{0.76}\text{N}_{0.18}\text{O}_{0.06}\text{H}_8$ by XPS (Figure 5e), while the converted SG contains tiny nitrogen (0.4 at%) and oxygen (1.4 at%). Accordingly, the high-binding-energy carbon components

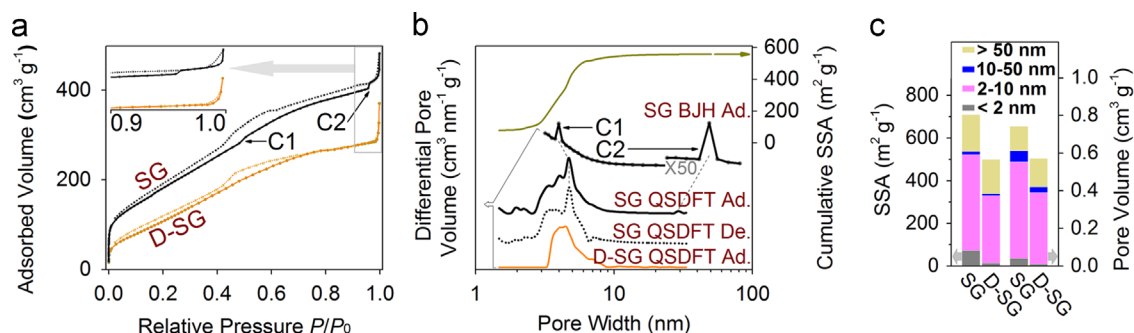


Figure 4 Surface area and porosity analyses of SG. (a) Nitrogen adsorption and desorption isotherms of SG and D-SG. C1 and C2 mark twice condensations only in SG. (b) Pore-size distribution of SG and D-SG, as well as QSDFT cumulative SSA of SG. (c) Partitioned SSA and specific pore volume based on QSDFT fitting, BET SSA and total pore volume near saturation vapor pressure.

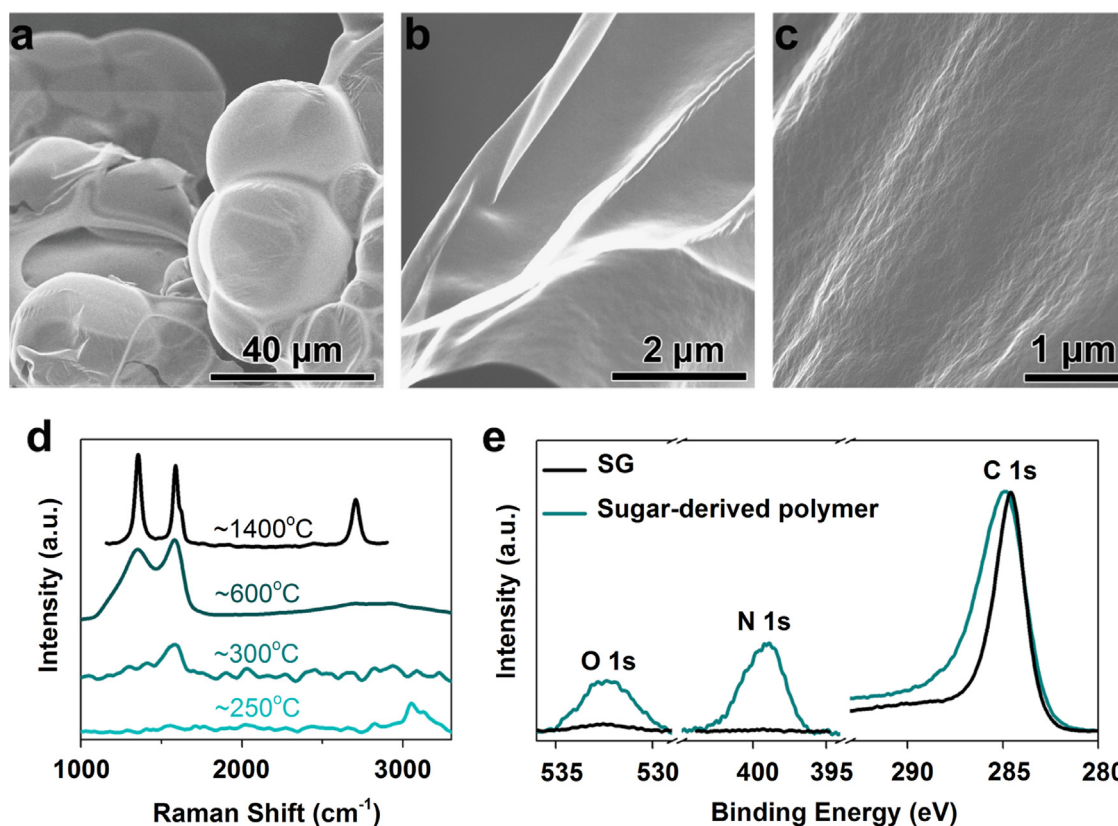


Figure 5 Intermediates in ammonium-assisted chemical blowing of sugars. (a-c) SEM images of the intermediate bubbles in the synthesis. (d) Evolution of Raman spectra of the intermediates and SG. (e) XPS of the intermediate taken around 300 °C and SG with calibration of gold internal standards.

relating to nitrogen/oxygen are completely removed to approach the standard graphite as shown in Figure 3c.

High-energy high-power supercapacitors based on SG

The excellent interconnection and specific porosity configuration of the SG enable its high performance EDLC. The SG-based supercapacitors using symmetric electrodes in an organic system demonstrate well capacitive electrical double layer (EDL) behavior with small ESR and large EPR as shown in the CV curves of Figure 6a. During galvanostatic constant-current charging/discharging (Figure 6b), the linear profiles correspond to a near-ideal capacitor. The capacitance approaches the intrinsic maximal value at low discharge current in principle when all accessible surfaces are utilized (Figure 6c), *ca.* 190 F g⁻¹, which results from the high SSA of SG. Along with increasing current density, the responsive surfaces decrease for the reduced penetration depth in pores due to distributed charge storage and sieving effect. The inner surfaces of micropores and mesopores sequentially become inaccessible, and the capacitances decay with increasing current (Figure 6c). Nevertheless, a capacitance of 58 F g⁻¹ is preserved at a very high current density of 100 A g⁻¹. The capacitance at the current density of 10 A g⁻¹ decreases to be 88% of the initial value after 1000 cycles, and then maintains at

113 F g⁻¹ for the next cycles, indicating the good electrochemical stability. The small current leakages and large EPR of the cell reveal the absence of micro-short-circuits (Figure 6d). The abnormal leakage currents at more than 1 V are caused by the electrolysis of impurities in agreement with CV curves.

The initial voltage drops of SG-based supercapacitors are proportional to the discharge currents (Figure 6e), determining the DC internal resistance around 2.5 Ω. The voltage drops become abnormal at too high or too low currents. The self-discharge may take account for the over voltage drops at designed currents comparable to the self-discharge current. In our opinion, the DC internal resistance calculated here is roughly 30% larger than ESR by analyzing the discharge curves of first several milliseconds. The voltage drops measured at 1.1 ms actually involve the additional components of electrochemical disturbance of ions when establishing stationary galvanostatic discharging in the initial period. The frequency-response behavior in Figure 6f exhibits a spike line at low frequency and a low line at high frequency region featuring the mixture control of distributed RC networks as well as ion diffusion. Alternate current internal resistance, normally defined as ESR, is 1.8 Ω. It includes the contact resistance of circuits, the electrolytic resistance between two electrodes and the intra-connection resistance of SG within electrodes. The third component is roughly estimated to be less than 1 Ω according to the method in the previous study [50],

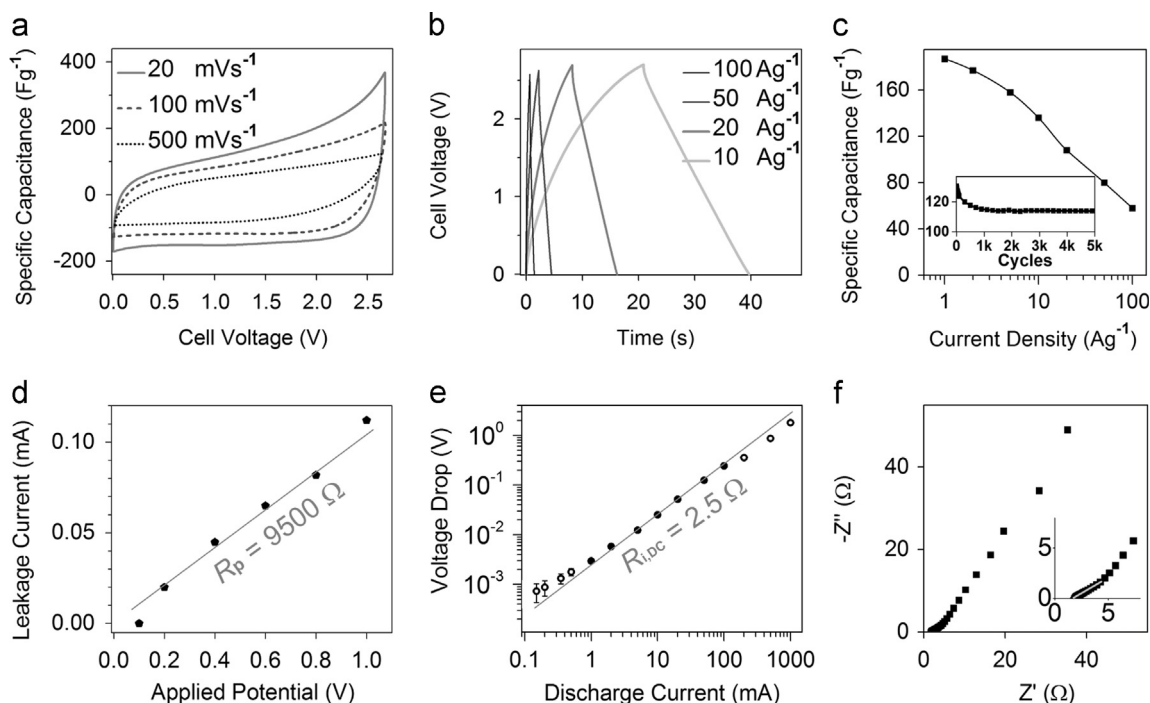


Figure 6 Performances of SG-based supercapacitors. (a) CV curves under different scan rates. (b) Galvanostatic charging/discharging plots over designed currents. (c) The change of specific capacitances along with discharge current density. The inset is the cycling performance at the current density of 10 A g^{-1} . (d) Leakage currents measured at different applied voltages. (e) Initial voltage drops measured at different galvanostatic discharge currents. (f) Nyquist plots for impedance analysis from EIS tests. The inset is a view of high frequency region.

reflecting the excellent interconnection of graphene membranes/struts for the high-speed transport of electrons.

The ionic and electronic transports lie at heart of supercapacitors. The breaches of SG would introduce enough inside continual channels for the smooth ion flow. The interconnected networks of SG provide the high way for electron transports. Combining such two factors, SG-based supercapacitors provide high capacitances at high currents with small internal resistances. They thus supply the high energy density of 50 Wh kg^{-1} comparable with Ni-MH batteries, and the high maximum-power density of 340 kW kg^{-1} (Figure 7). Comparing with our previous aqueous supercapacitors, the energy density in the organic supercapacitors is improved by one magnitude order due to the higher operation voltage, while the power density is maintained at high levels due to small internal resistances. The interconnected membranes and struts, appropriate porosity of SG and the removal of additives and binders contribute to such minimized internal resistance. The SG electrodes require neither additional 3D fabrication nor polymer binders nor conductive additives, beneficial for practical manufactures. The overall performance of SG-based supercapacitors ranks within the top level of the reports for 3D graphene supercapacitors with a 2.7 V operation voltage, which are attractive for the electricity storage/release for the quick start-up of electric vehicles and for shaving day-night power fluctuations.

Conclusion

In summary, a general concept of synthesis protocols, ammonium-assisted chemical blowing, is established to

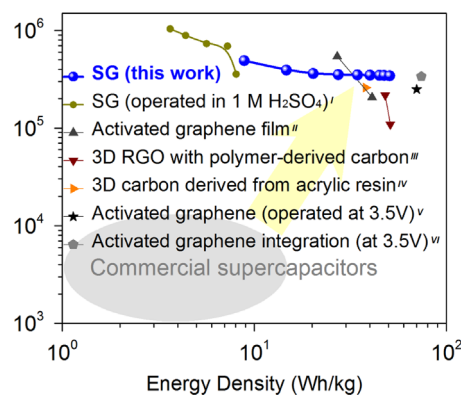


Figure 7 Ragone plot of SG-based supercapacitors comparing with other 3D graphene organic supercapacitors. I is extracted from Ref. [50] as a reference operated in $1 \text{ M H}_2\text{SO}_4$; II and III were operated in $1 \text{ M TEABF}_4/\text{AN}$ extracted from Ref. [60,61] respectively; IV was operated in $1 \text{ M TEABF}_4/\text{propylene carbonate}$ from Ref. [62]; V was operated in $\text{BMIMBF}_4/\text{AN}$ from Ref. [63]; VI was operated in $[\text{EMIM}][\text{TFSI}]/\text{AN}$ from Ref. [64].

reliably produce the SG on a large scale, which enriches the methodology for preparing 3D graphenes. The SG has good interconnectivity, large SSA and appropriate porosity. Based on these structures, their supercapacitors demonstrate the high energy density and the high power density. The easy production and high-performance supercapacitors of SG will enable the extensive potential applications of graphenes.

Acknowledgments

This work was supported by KAKENHI projects (Grant-in-Aid for Young Scientists, 26820322 and 15K18216), International Center for Young Scientists (ICYS), and World Premier International Research Center (WPI) initiative on Materials Nanoarchitectonics (MANA) from Japan Society for the Promotion of Science (JSPS), and Ministry of Education, Culture, Sports, Science & Technology (MEXT) in Japan. X.F. J. and X.B.W. thank Drs. K. Miyano, M. Mitome, Y. Ide, A. Nukui, N. Kawamoto and Ms. K. Takahashi for experimental assistances and discussions.

References

- [1] P. Simon, Y. Gogotsi, *Nat. Mater.* 7 (2008) 845-854.
- [2] W.Y. Tsai, R.Y. Lin, S. Murali, L.L. Zhang, J.K. McDonough, R.S. Ruoff, P.L. Taberna, Y. Gogotsi, P. Simon, *Nano Energy* 2 (2013) 403-411.
- [3] S.Y. Yin, Z.Q. Niu, X.D. Chen, *Small* 8 (2012) 2458-2463.
- [4] X.H. Cao, Z.Y. Yin, H. Zhang, *Energy Environ. Sci.* 7 (2014) 1850-1865.
- [5] R.T. Lv, E. Cruz-Silva, M. Terrones, *ACS Nano* 8 (2014) 4061-4069.
- [6] Y.X. Xu, K.X. Sheng, C. Li, G.Q. Shi, *ACS Nano* 4 (2010) 4324-4330.
- [7] Z.S. Wu, A. Winter, L. Chen, Y. Sun, A. Turchanin, X.L. Feng, K. Mullen, *Adv. Mater.* 24 (2012) 5130-5135.
- [8] P. Chen, J.J. Yang, S.S. Li, Z. Wang, T.Y. Xiao, Y.H. Qian, S.H. Yu, *Nano Energy* 2 (2013) 249-256.
- [9] U.N. Maiti, J. Lim, K.E. Lee, W.J. Lee, S.O. Kim, *Adv. Mater.* 26 (2014) 615-619.
- [10] J.L. Vickery, A.J. Patil, S. Mann, *Adv. Mater.* 21 (2009) 2180-2184.
- [11] H.Y. Sun, Z. Xu, C. Gao, *Adv. Mater.* 25 (2013) 2554-2560.
- [12] L. Qiu, J.Z. Liu, S.L.Y. Chang, Y.Z. Wu, D. Li, *Nat. Commun.* 3 (2012) 1241.
- [13] X.W. Yang, C. Cheng, Y.F. Wang, L. Qiu, D. Li, *Science* 341 (2013) 534-537.
- [14] S. Korkut, J.D. Roy-Mayhew, D.M. Dabbs, D.L. Milius, I.A. Aksay, *ACS Nano* 5 (2011) 5214-5222.
- [15] Y.X. Xu, Z.Y. Lin, X.Q. Huang, Y. Liu, Y. Huang, X.F. Duan, *ACS Nano* 7 (2013) 4042-4049.
- [16] X.W. Yang, J.W. Zhu, L. Qiu, D. Li, *Adv. Mater.* 23 (2011) 2833-2838.
- [17] X. Yang, L. Qiu, C. Cheng, Y. Wu, Z.F. Ma, D. Li, *Angew. Chem. Int. Ed.* 50 (2011) 7325-7328.
- [18] Z.Q. Niu, J. Chen, H.H. Hng, J. Ma, X.D. Chen, *Adv. Mater.* 24 (2012) 4144-4150.
- [19] S.H. Lee, H.W. Kim, J.O. Hwang, W.J. Lee, J. Kwon, C.W. Bielawski, R.S. Ruoff, S.O. Kim, *Angew. Chem. Int. Ed.* 49 (2010) 10084-10088.
- [20] T. Nathan-Walteser, I.M. Lazar, M. Fabritius, F.J. Tolle, Q. Xia, B. Bruchmann, S.S. Venkataraman, M.G. Schwab, R. Mulhaupt, *Adv. Funct. Mater.* 24 (2014) 4706-4716.
- [21] C. Zhu, T.Y. Han, E.B. Duoss, A.M. Golobic, J.D. Kuntz, C.M. Spadaccini, M.A. Worsley, *Nat. Commun.* 6 (2015) 6962.
- [22] B.G. Choi, M. Yang, W.H. Hong, J.W. Choi, Y.S. Huh, *ACS Nano* 6 (2012) 4020-4028.
- [23] Z.L. Wang, D. Xu, H.G. Wang, Z. Wu, X.B. Zhang, *ACS Nano* 7 (2013) 2422-2430.
- [24] C.M. Chen, Q. Zhang, C.H. Huang, X.C. Zhao, B.S. Zhang, Q. Q. Kong, M.Z. Wang, Y.G. Yang, R. Cai, D.S. Su, *Chem. Commun.* 48 (2012) 7149-7151.
- [25] X.D. Huang, K. Qian, J. Yang, J. Zhang, L. Li, C.Z. Yu, D.Y. Zhao, *Adv. Mater.* 24 (2012) 4419-4423.
- [26] P.M. Sudeep, T.N. Narayanan, A. Ganesan, M.M. Shaijumon, H. Yang, S. Ozden, P.K. Patra, M. Pasquali, R. Vajtai, S. Ganguli, A.K. Roy, M.R. Anantharaman, P.M. Ajayan, *ACS Nano* 7 (2013) 7034-7040.
- [27] Y. Zhao, C.G. Hu, Y. Hu, H.H. Cheng, G.Q. Shi, L.T. Qu, *Angew. Chem. Int. Ed.* 51 (2012) 11371-11375.
- [28] Y. Zhao, J. Liu, Y. Hu, H.H. Cheng, C.G. Hu, C.C. Jiang, L. Jiang, A.Y. Cao, L.T. Qu, *Adv. Mater.* 25 (2013) 591-595.
- [29] Z.H. Tang, S.L. Shen, J. Zhuang, X. Wang, *Angew. Chem. Int. Ed.* 49 (2010) 4603-4607.
- [30] H.P. Cong, X.C. Ren, P. Wang, S.H. Yu, *ACS Nano* 6 (2012) 2693-2703.
- [31] Z.S. Wu, S.B. Yang, Y. Sun, K. Parvez, X.L. Feng, K. Mullen, *J. Am. Chem. Soc.* 134 (2012) 9082-9085.
- [32] J. Chen, K.X. Sheng, P.H. Luo, C. Li, G.Q. Shi, *Adv. Mater.* 24 (2012) 4569-4573.
- [33] Z.L. Wang, D. Xu, J.J. Xu, L.L. Zhang, X.B. Zhang, *Adv. Funct. Mater.* 22 (2012) 3699-3705.
- [34] V.C. Tung, L.M. Chen, M.J. Allen, J.K. Wassei, K. Nelson, R.B. Kaner, Y. Yang, *Nano. Lett.* 9 (2009) 1949-1955.
- [35] Z.J. Fan, J. Yan, L.J. Zhi, Q. Zhang, T. Wei, J. Feng, M. L. Zhang, W.Z. Qian, F. Wei, *Adv. Mater.* 22 (2010) 3723-3728.
- [36] Y.W. Cheng, S.T. Lu, H.B. Zhang, C.V. Varanasi, J. Liu, *Nano Lett.* 12 (2012) 4206-4211.
- [37] Y.P. Wu, T.F. Zhang, F. Zhang, Y. Wang, Y.F. Ma, Y. Huang, Y. Y. Liu, Y.S. Chen, *Nano Energy* 1 (2012) 820-827.
- [38] S. Nardecchia, D. Carriazo, M.L. Ferrer, M.C. Gutierrez, F. del Monte, *Chem. Soc. Rev.* 42 (2013) 794-830.
- [39] W. Wang, S.R. Guo, M. Penchev, I. Ruiz, K.N. Bozhilov, D. Yan, M. Ozkan, C.S. Ozkan, *Nano Energy* 2 (2013) 294-303.
- [40] D.T. Pham, T.H. Lee, D.H. Luong, F. Yao, A. Ghosh, V.T. Le, T. H. Kim, B. Li, J. Chang, Y.H. Lee, *ACS Nano* 9 (2015) 2018-2027.
- [41] L.L. Jiang, L.Z. Sheng, C.L. Long, Z.J. Fan, *Nano Energy* 11 (2015) 471-480.
- [42] J. Yan, Q. Wang, C. Lin, T. Wei, Z.J. Fan, *Adv. Energy Mater.* 4 (2014) 1400500.
- [43] Z.B. Lei, N. Christov, X.S. Zhao, *Energy Environ. Sci.* 4 (2011) 1866-1873.
- [44] R.L. Liu, L. Wan, S.Q. Liu, L.X. Pan, D.Q. Wu, D.Y. Zhao, *Adv. Funct. Mater.* 25 (2015) 526-533.
- [45] X. Li, X.B. Zang, Z. Li, X.M. Li, P.X. Li, P.Z. Sun, X. Lee, R.J. Zhang, Z.H. Huang, K.L. Wang, D.H. Wu, F.Y. Kang, H.W. Zhu, *Adv. Funct. Mater.* 23 (2013) 4862-4869.
- [46] S.Y. Wang, B. Pei, X.S. Zhao, R.A.W. Dryfe, *Nano Energy* 2 (2013) 530-536.
- [47] Z.P. Chen, W.C. Ren, L.B. Gao, B.L. Liu, S.F. Pei, H.M. Cheng, *Nat. Mater.* 10 (2011) 424-428.
- [48] X. Cao, Y. Shi, W. Shi, G. Lu, X. Huang, Q. Yan, Q. Zhang, H. Zhang, *Small* 7 (2011) 3163-3168.
- [49] X. Xiao, T.E. Beechem, M.T. Brumbach, T.N. Lambert, D.J. Davis, J.R. Michael, C.M. Washburn, J. Wang, S. M. Brozik, D.R. Wheeler, D.B. Burckel, R. Polsky, *ACS Nano* 6 (2012) 3573-3579.
- [50] X.B. Wang, Y.J. Zhang, C.Y. Zhi, X. Wang, D.M. Tang, Y.B. Xu, Q.H. Weng, X.F. Jiang, M. Mitome, D. Golberg, Y. Bando, *Nat. Commun.* 4 (2013) 2905.
- [51] X.B. Wang, C.Y. Zhi, L. Li, H.B. Zeng, C. Li, M. Mitome, D. Golberg, Y. Bando, *Adv. Mater.* 23 (2011) 4072-4076.
- [52] A.C. Ferrari, J.C. Meyer, V. Scardaci, C. Casiraghi, M. Lazzeri, F. Mauri, S. Piscanec, D. Jiang, K.S. Novoselov, S. Roth, A.K. Geim, *Phys. Rev. Lett.* 97 (2006) 187401.
- [53] E. Yoo, J. Kim, E. Hosono, H.S. Zhou, T. Kudo, I. Honma, *Nano Lett.* 8 (2008) 2277-2282.
- [54] J. Yan, W.Y. Ruan, M.Y. Chou, *Phys. Rev. B* 77 (2008) 125401.
- [55] R.A. Rosenberg, P.J. Love, V. Rehn, *Phys. Rev. B* 33 (1986) 4034.

- [56] J.J. Cuomo, J.P. Doyle, J. Bruley, J.C. Liu, Appl. Phys. Lett. 58 (1991) 466-468.
- [57] S.Y. Li, H.H. Zhou, J.L. Gu, J. Zhu, Carbon 38 (2000) 929-941.
- [58] T. Takahagi, A. Ishitani, Carbon 26 (1988) 389-395.
- [59] H. Hatori, Y. Yamada, M. Shiraishi, Carbon 31 (1993) 1307-1312.
- [60] L.L. Zhang, X. Zhao, M.D. Stoller, Y.W. Zhu, H.X. Ji, S. Murali, Y.P. Wu, S. Perales, B. Clevenger, R.S. Ruoff, Nano Lett. 12 (2012) 1806-1812.
- [61] L. Zhang, F. Zhang, X. Yang, G.K. Long, Y.P. Wu, T.F. Zhang, K. Leng, Y. Huang, Y.F. Ma, A. Yu, Y.S. Chen, Sci. Rep. 3 (2013) 1408.
- [62] Y.Y. Li, Z.S. Li, P.K. Shen, Adv. Mater. 25 (2013) 2474-2480.
- [63] Y.W. Zhu, S. Murali, M.D. Stoller, K.J. Ganesh, W.W. Cai, P.J. Ferreira, A. Pirkle, R.M. Wallace, K.A. Cychosz, M. Thommes, D. Su, E.A. Stach, R.S. Ruoff, Science 332 (2011) 1537-1541.
- [64] T. Kim, G. Jung, S. Yoo, K.S. Suh, R.S. Ruoff, ACS Nano 7 (2013) 6899-6905.



Xiang-Fen Jiang received her M.S. degree from Nanjing University in 2009 and Ph.D. degree from Waseda University in 2013, working on hierarchically nanostructured nitrogen-doped carbon and ordered mesoporous metal oxide thin films, respectively. Since October 2013, she has joined the group of Prof. Yoshio Bando as a postdoc in the International Center for Materials Nanoarchitectonics (MANA) of National Institute for Materials Science (NIMS). Her current research interest is synthesizing porous structures of boron nitride nanosheets for environmental science and carbon-based nanosheets for energy conversion.



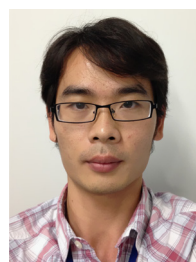
Xue-Bin Wang received his B.S. and M.S. degrees from Nanjing University in China, and got his Ph.D. degree from Waseda University in Japan in 2013. He worked as Junior Researcher (2010-2013) and Postdoc Researcher (2013-2014) in National Institute for Materials Science (NIMS). He has worked as ICYS Researcher in World Premier International Center for Materials Nanoarchitectonics (WPI-MANA) and NIMS since 2014. He has been pursuing the designed synthesis, novel properties and practical applications of low-dimensional functional materials. His research recently focuses on the growth of 3D-designed nanosheets, such as strutted-graphene and BN nanosheets, and their applications to supercapacitors, polymeric composites *etc.*



Pengcheng Dai received his B.S. and Ph.D. degrees in School of Chemistry and Chemical Engineering, Shandong University, China, in 2009 and 2014, respectively, under the supervision of Prof. Jinhua Zhan, mainly working on photoelectrochemical solar cells. During 2012 to 2014, he worked as a visiting scholar in Boston College (USA) on solar water splitting. He is now a postdoctoral researcher in Prof. Yoshio Bando's group at the National Institute for Materials Science (NIMS). His current research focuses nanostructured materials for energy conversion and pollutant detection.



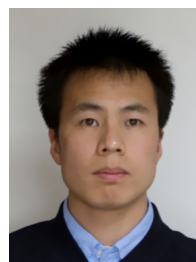
Xia Li obtained her Ph.D. degree in material physics and chemistry in 2007 from Shanghai Institute of Ceramics, Chinese Academy of Sciences (SICCAS). From 2007 to 2012 she was a postdoctoral researcher and then a JSPS postdoctoral fellow at the National Institute of Advanced Industrial Science and Technology (AIST), Japan. Afterwards, she joined the National Institute for Materials Science (NIMS), Japan, as a MANA research associate. Her research interests focus on synthesis, characterization and biomedical application of inorganic materials.



Qunhong Weng received his B.S. and M.S. degree in Chemistry from Huazhong Agricultural University (2007) and Xiamen University (2010), respectively. In March 2015, he obtained his Ph.D. degree in Material Science and Engineering from University of Tsukuba under the supervision of Prof. Dmitri Golberg. Now, he is a MANA postdoctoral researcher of Prof. Yoshio Bando's group at National Institute for Materials Science (NIMS). His research focuses on functionalized layered materials for clean energy storage and conversion applications.



Xi Wang obtained his Ph.D. degree in physical chemistry from the Institute of Chemistry, Chinese Academy of Sciences (ICCAS). He was a Japan Society for the Promotion of Science (JSPS) postdoctoral fellow and now is an ICYS Researcher in National Institute for Materials Science (NIMS). His current research topic is the controlled fabrication, novel properties and optoelectronic applications of semiconductor nanostructures, with a special focus on hollow structure-based energy applications.



Dai-Ming Tang received his Ph.D. in materials science in 2010 from the Institute of Metal Research (IMR), Chinese Academy of Sciences (CAS). Currently he is a permanent researcher & MANA scientist at International Center for Materials Nanoarchitectonics (MANA), National Institute for Materials Science (NIMS), Japan. His research interest is to understand structure-properties relationship and design new materials at multi-scales.



Jie Tang is the group leader of the One-Dimensional Nanomaterials Group and senior research scientist in the National Institute for Materials Science in Tsukuba, Japan. She received her B.S. degree from Tsinghua University, China, and Ph.D. degree in physics from Osaka University, Japan. She is also an adjunct professor of physics in the University of North Carolina at Chapel Hill, USA. Her recent research focuses on synthesis, characterization and applications of low-dimensional nanomaterials including graphene supercapacitors and rare-earth boride nanowires as molecular probes and point electron emitters as well as their materials properties under high pressure.



Yoshio Bando received his Ph.D. degree from Osaka University in 1975 and joined the National Institute for Research in Inorganic Materials (at present NIMS) in the same year. From 1979 to 1981 he worked as a visiting researcher at Arizona State University. Currently, he is a Chief Operating Officer (COO) of the International Center for Materials Nanoarchitectonics (MANA) and a Fellow within the National Institute for Materials Science (NIMS). He is also a visiting Professor at Waseda University. His current research concentrates on the synthesis and properties of various inorganic nanostructures and their TEM characterizations. He has published more than 600 papers in international journals and the total number of citations of his papers is over 27,000. The H-index of his publications is 86. He received the 16th Tsukuba Prize in 2005 for his studies on novel inorganic nanotubes and nanothermometers and the 2011 Thomson Reuters Research Front Award for his investigations on 1D-nanostructures.



Dmitri Golberg joined NIMS in 1995. At present, he is a Nanotube Unit Director of MANA-NIMS and Professor of University of Tsukuba. To date, Dmitri has authored more than 550 original papers in peer-reviewed International journals and over 100 Japanese and International patents. His numerous scientific awards include Tsukuba Prize, "Thomson Reuters" Research Front Award and "Seto Award" from the Japanese Microscopy Society for developments of *in situ* TEM techniques. Dmitri is listed among top-150 highly-cited world materials scientists by "Thomson Reuters". His works have been cited more than 21000 times and H-factor of his publications is 76.